Surface hydrogenation of oxygen terminated MXenes M_2CO_2 (M = Ti, V, Nb)

Tatyana R. Kayumova[a,*], Ilay P. Kolganov[a], Alexander V. Myshlyavtsev[a], Pavel V. Stishenko[a,b], Anastasiia I. Fadeeva[a]

[a] *Omsk State Technical University, 11 Mira, Omsk 644050, Russian Federation*
[b] *Cardiff Catalysis Institute, School of Chemistry, Cardiff University, Cardiff, United Kingdom*

ARTICLE INFO

Keywords:
MXenes
Functional groups
Hydrogenation
DFT
Monte Carlo simulation

ABSTRACT

We have investigated reduction of MXenes M_2CO_2 (M = Ti, V, Nb) surface by hydrogen using density functional theory and statistical physics methods. We have approximated lateral interactions between adsorbed hydrogen with simple pairwise potential. We have confirmed model stability via cross-validation. Adsorption isotherms are calculated using Metropolis Monte Carlo method. We have built analytical Langmuir-like approximation of calculated isotherms. Ordered phases with 1/3 and 2/3 ML coverage are visually observed at low temperatures. At temperatures above 300 K no obvious plateau is observed, and intermediate phases does not exist. We compared adsorptive properties of MXenes at the same external conditions.

1. Introduction

Recently, two-dimensional (2D) metal carbides, nitrides and carbonitrides, the so-called MXenes, attracted great interest due to their unique properties namely: universal composition and structure, stability under certain conditions, hydrophilicity, electronic conductivity [1], high surface area [2], surface functionality [3]. Most MXenes are obtained by selective etching of atomic layers from MAX-phases [4,5]. Due to its unique properties MXenes are of prospective use as Mg-ion and Li-ion batteries [6-9], sensors [10], catalysts for hydrogen production [11], water dissociation [12], ammonia synthesis [13], nitrogen reduction reactions [14], etc.

During MXenes synthesis, functional groups T = (OH, O, F) are adsorbed onto the surface. Functional groups contribute greatly to the properties of MXenes. Surface terminations affect thermodynamics, stability in MXenes surface applications [15-19]. Using an electric field in the work [1] changed the conductivity and magnetic properties of the Ti_2C monolayer. This opens broad prospects for the use of nanomagnetic electronic devices. Understanding MXenes surface termination and their stability is critical for adapting these materials to specific applications [20].

Experiments show that fluorine can be removed from MXenes by heating up to temperature of 750 ^oC [21]. For many applications' fluorine is not present in working environment, therefore we can assume that once cleared MXenes surface will not have fluorine terminations at operation conditions.

Experiments have shown [4] that oxygen terminations are stable at least up to 1400 K. Calculations predict [22] that full oxygen coverage is thermodynamically favourable even at very high temperature 2700 K at partial pressure of 10^{-9} bar. Therefore, it is very difficult to create such conditions that oxygen will not be on the surface. So, for most applications of MXenes we should assume full oxygen coverage.

Hydrogen tend to adsorb on oxygenated MXenes forming OH terminations. Whilst hydrogen binds much weaker than oxygen or even fluorine and can be removed if necessary, it is ubiquitous in nature and prospective application environments. Therefore, it's presence and concentration on surface is in thermodynamic equilibrium and depends on environment temperature, partial pressure, or generally on chemical potential of hydrogen.

Here we considered three MXenes with general formula M_2CO_2 (M = Ti, V, Nb). These MXenes are synthesizable [4] and are extensively researched for a number of applications [23-25]. We have revelled thermodynamic behaviour of hydrogen adlayer on these MXenes. Parameters of lateral interactions between adsorbed hydrogen adatoms were estimated via DFT calculation. Adsorption isotherms were calculated within lattice model framework using parallel replica Metropolis Monte Carlo method. Simulated isotherms were approximated with analytical expressions.

* Corresponding author.
E-mail address: t_kaumova36@mail.ru (T.R. Kayumova).

2. Computation details

The calculations were performed in the Quantum Espresso [26] and SuSMoST [27] software packages. For DFT calculations the PBE functional was used with Grimme-D3 corrections [28]. The cut-off energy was fitted to convergence of total energy with 0.01 eV accuracy. The cutoff energies for Ti_2CO_2- H, Nb_2CO_2- H, and V_2CO_2- H were 707 eV, 775 eV, and 802 eV, respectively. The distance between the MXene layers was 12 Å to avoid interactions of periodic images. Size of simulated structures varied from 1 to 9 unit cells of an empty MXene sheet. Hydrogen coverage varied from 1/9 to full coverage (1 ML), when each oxygen atom on the surface had a hydrogen atom on it. Geometry relaxation of all structures was performed to reach maximal force below 0.0001 eV/Ang (see Supplementary Information: out-file of DFT calculation). Fig. 1 shows images of the geometry-optimized MXenes M_2CO_2 - H (M = Ti, V, Nb) configurations.

Obtained total energies were approximated by pairwise Hamiltonian (1).

$$H_i = uS_i + \mu N_i + \sum_{j=1}^{p} k_{ij}\phi\, r_j \qquad (1)$$

Here H_i is the total potential energy of the i th structure, u is energy of the empty MXene unit cell, S_i is size of i th structure in unit cells, μ is energy of the hydrogen adsorption complex in the limit of zero coverage, N_i is the number of adsorbed hydrogen atoms, p is the number of coordination spheres of the surface lattice with considered lateral interactions, r_j is the radius of j-th coordination sphere, k_{ij} is number of hydrogen pairs at r_j distance in i th structure, Φ is the function of lateral interactions. Φ is tabulated due to discreteness of its argument. Values of u, μ, and Φ were fitted to DFT computed energies using least squares method (2).

$$(u, \mu, \phi) = \underset{u,\mu,\phi}{argmin} \sum_{i=1}^{n} (D_i - H_i(u, \mu, \phi))^2 \qquad (2)$$

Here D_i is the total energy of i th structure calculated with DFT, n is the number of DFT calculated structures (n = 29 for Ti_2CO_2, n = 31 for V_2CO_2 and Nb_2CO_2). To ensure stability of this parameterization and check Hamiltonian accuracy we employed cross-validation technique (CV), particularly leave-5-out CV. For each considered MXene we divided its set of DFT computed structures into validation subset of size t = 5 and training subset of size n - t. All t-combinations of n structures were considered. Total number of combinations for each MXene was equal to binomial coefficient C_{tn} (118,755 for Ti_2CO_2 and 169,911 for V_2CO_2 and Nb_2CO_2). For each CV combination values of u, μ, and Φ were fitted to energies of a training subset:

$$u_j, \mu_j, \phi_j = \underset{u,\mu,\phi}{argmin} \sum_{i \in T_j} (D_i - H_i(u, \mu, \phi))^2 \qquad (3)$$

Here j is index of CV combination ($1 \le j \le C_{tn}$), T_j is training subset of j-th combination, u_j, μ_j, and Φ_j are Hamiltonian parameters fitted to subset T_j of DFT calculated structures. To estimate stability of parameters fitting (2) we calculated mean values and standard deviations of the same parameters over CV fittings (3). See Table 1 for obtained values. To estimate accuracy of the obtained Hamiltonian we calculated maximums of absolute error per unit cell over validation subsets (4), these values are also in Table 1.

$$MaxAE_j = \max_{i \in \Omega \setminus T_j} \left| \frac{D_i - H_i(u_j, \mu_j, \phi_j)}{S_i} \right| \qquad (4)$$

Here j is index of CV combination ($1 \le j \le C_{tn}$), Ω is a total set of DFT calculated structures. Adsorption isotherms were simulated using the obtained Hamiltonian by means of Parallel Tempering Monte Carlo simulations. Simulations were carried out in the framework of the lattice model [27] using the SuSMoST software package at temperatures from 25 K to 500 K. Simulations were performed on lattices with a linear size L = 60. A 100,000 Monte Carlo steps were used to bring the system into equilibrium followed by another 50,000 steps to calculate the averaged characteristics.

3. Results and discussion

3.1. Model Hamiltonian

Hamiltonian fitting results are summarized in Table 1. The following features are common for all considered MXenes:

1 Standard deviations of fitted parameters over cross-validation subsets are of the units of meV scale, that is much smaller than values of parameters itself almost in all cases. Therefore, we consider the Hamiltonian parameterization as stable and rule out overfitting risk.
2 Maximum abolute errors (MaxAE) in all cases are of the order of 10 meV and less than so called chemical accuracy 1 kcal/mol.

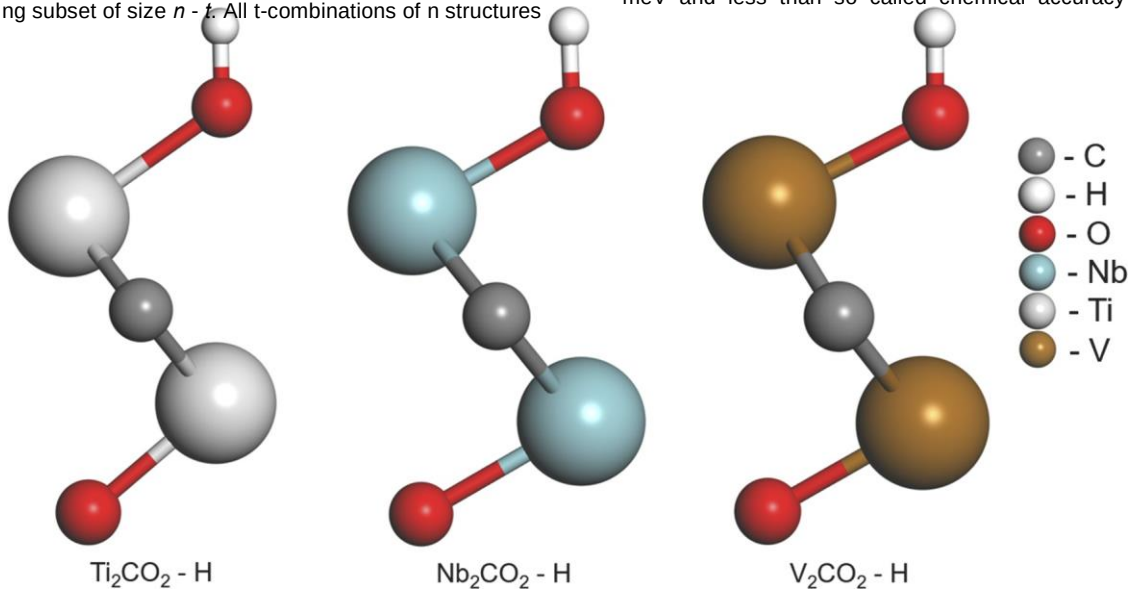

Fig. 1. Geometry-optimized MXenes M_2CO_2 - H (M = Ti, V, Nb) configurations.

Table 1
Parameters of the Hamiltonian of hydrogen adlayer on M_2CO_2 MXenes fitted to DFT calculations with, errors and cross-validation (CV) results. $E_{H\text{-}mol}$, = 15.85225 eV is a hydrogen atom energy in H_2 molecule, u_{ref} is the energy of the empty MXene unit cell calculated by the density functional theory method.

Structure		r/a_0	Total DFT set fit	CV fit mean	CV fit standard deviation
Ti_2CO_2- H u_{ref} = 4208.75059 eV a_0 = 3.014 Å	u - u_{ref}, meV	21.47	22.57	4.97	
	$\mu_{ads} = \mu$ - $E_{H\text{-}mol}$, meV	636.33	634.21	15.5	
	Φ, meV	1	118.8	119.29	5.15
		$\sqrt{3}$	31.26	30.53	6.71
		2	41.62	41.85	2.51
		$\sqrt{7}$	19.33	19.21	1.77
	MaxAE, meV	21.47	10.87	6.98	
V_2CO_2-H u_{ref} = 4942.95771 eV a_0 = 2.891 Å	u - u_{ref}, meV	6.05	6.18	1.67	
	$\mu_{ads} = \mu$ - $E_{H\text{-}mol}$, meV	739.46	739.5	7.52	
	Φ, meV	1	144.4	144.61	2.5
		$\sqrt{3}$	2.52	2.45	2.54
		2	34.6	34.66	1.63
		$\sqrt{7}$	12.58	12.57	0.93
	MaxAE, meV	8.96	9.26	3.55	
Nb_2CO_2-H u_{ref} = 4241.79793 eV a_0 = 3.099 Å	u - u_{ref}, meV	5.13	5.31	1.04	
	$\mu_{ads} = \mu$ - $E_{H\text{-}mol}$, meV	115.11	114.05	5.77	
	Φ, meV	1	94.07	93.95	2.06
		$\sqrt{3}$	13.51	13.6	2.2
		2	14.31	14.19	1.21
		$\sqrt{7}$	3.71	3.57	0.72
	MaxAE, meV	6.79	6.43	3.71	

Therefore, the obtained model with its parameterization is sufficiently accurate for chemical applications.

3 Lateral interactions between hydrogen adatoms are always repulsive. First-neighbour interactions $\Phi(a_0)$ negatively correlate with the lattice parameter a_0 being strongest for vanadium and the weakest for niobium. Repulsion energy generally decay with distance, but between second-nearest neighbours Φ ($\sqrt{3}a_0$) it is always weaker than between third-nearest neighbours $\Phi(2a_0)$. We suppose that this is due to peculiarities of charge distribution and screening effects. Similar effect was observed for oxygen adatoms on V_2C MXene [22].

Some peculiarities were observed for specific MXenes. DFT calculations converged much slower for Ti_2CO_2 than for Nb_2CO_2 and V_2CO_2. Therefore, we managed to compute only 29 structures for titanium within available computational budget. Whilst for niobium and vanadium we got 31 ones.

Also, for titanium MaxAE and standard deviations of Hamiltonian parameters over CV samples were approximately twice larger than for other considered metals, but still within chemical accuracy.

It is notable, that for Nb_2CO_2 parameter μ is much smaller than for Ti_2CO_2 or V_2CO_2. In Table 1 μ_{ads} is an adsorption energy relative to energy of molecular hydrogen, hence these values are essentially adsorption energies at T = 0 K, when entropic contributions are absent.

3.2. Statistical adlayer simulations

Surface coverage isotherms are shown in Fig. 2 along with simulated adlayer snapshots (see Supplementary Information: Monte-Carlo simulation models). The isotherms show plateaus at coverages θ = 0, 1/3, 2/3, and 1 hydrogen monolayer (ML). Plateaus at θ =1/3 ML and θ =2/3 ML correspond to ordered phases with $\sqrt{3} \times \sqrt{3}\ R60^\circ$ unit cell. Corresponding simulated lattice snapshots are in plot insets in Fig. 2. These phases are well known to exist in adsorption models on triangular lattices with finite nearest-neighbour repulsions (for example see Fig. 4 (a) in [29] or Table 1 in [30]). This result was expected due to dominating magnitude of $\Phi(a_0)$ in lateral interactions of the Hamiltonian. This is consistent with the study by Zhan et al. [31], who also observe hydrogen coverage of 1/3 and 2/3 ML on Ti_3C_2 at different values of the electrode potential. In [20] Ibragimova, Puska, and Komsa also observes phase 2/3 ML on Ti_2C (see Supporting Information, Fig. S7). They also described the ½ ML phase, that we didn't observe, probably because we considered grand canonical ensemble that do not fix amount of adsorbate species, whilst it was noted [20] that surface with such a coverage is very sensitive to changes in external factors and it is hard to fully predict the composition of this phase. Perhaps it is possible to obtain ½ ML phase at very low temperature in a narrow range of chemical potential, but it is out of scope of this study. The snapshots of 1/3 and 2/3 ML phases in insets in Fig. 2 are taken from simulations at a temperature of 50 K. Ordered phases with 1/3 and 2/3 ML coverage are visually observed at low temperatures. At temperatures above 300 K no obvious plateau is observed, and intermediate phases does not exist. Ranges of these phases existence are different for considered MXenes. For Nb_2CO_2 it is considerably smaller than for Ti_2CO_2 or V_2CO_2, that can be associated with lower energies of lateral interactions for H adatoms on Nb_2CO_2.

Fig. 2(d) shows adoption isotherms shifted on the ground-state binding energy μ_{ads} for comparison of adsorptive properties of MXenes at the same external conditions. One can see that at room temperature vanadium coverage is always the highest one, and for niobium it is the lowest. From ideal gas approximation it follows that at temperature T = 273 K free energy of hydrogen in molecular form is about 150 meV per atom at pressure P = 1 atm and is about 300 meV at $P = 0.5 \cdot 10^6$ atm (partial pressure of molecular hydrogen in atmospheric air [32]). At these conditions hydrogen coverage is almost zero for niobium, 1/3 ML for titanium, and a bit more than 1/3 ML for vanadium.

3.3. Adsorption isotherms

Pairwise Hamiltonian (1) is symmetric with respect to exchange of occupied and unoccupied lattice sites. Consequently, all obtained isotherms are symmetric with respect to θ =1/2 ML point. In particular:

$$\theta(\lambda + \mu) = 1 \qquad \theta(\lambda \qquad \mu) \tag{5}$$

Here λ is the energy of lateral interactions at full coverage. So $\theta(-\lambda) = 1/2\ ML$ is the symmetry point.

We approximated obtained adsorption isotherms with a sum of shifted and scaled Langmuir isotherms satisfying (5) property.

$$_{kB}{}^{T} \tag{6}$$

$$\theta_L(\mu) = \frac{W(\mu)}{1 + W(\mu)} \tag{7}$$

$$\theta(\mu) = \frac{\theta_L(A(\mu + \lambda \quad s)) + \theta_L(A(\mu + \lambda)) + \theta_L(A(\mu + \lambda + s))}{3} \tag{8}$$

Here W is a Boltzmann weight function, $\theta_L(\mu)$ is a Langmuir isotherm, A is a scaling coefficient, s is a shifting coefficient. See Table 2 for obtained isotherm's parameters.

Parameter A describes thermal stability of ordered phases, while parameter s characterizes width of chemical potential range of intermediate coverage phases. Values of A and s were fitted to calculated

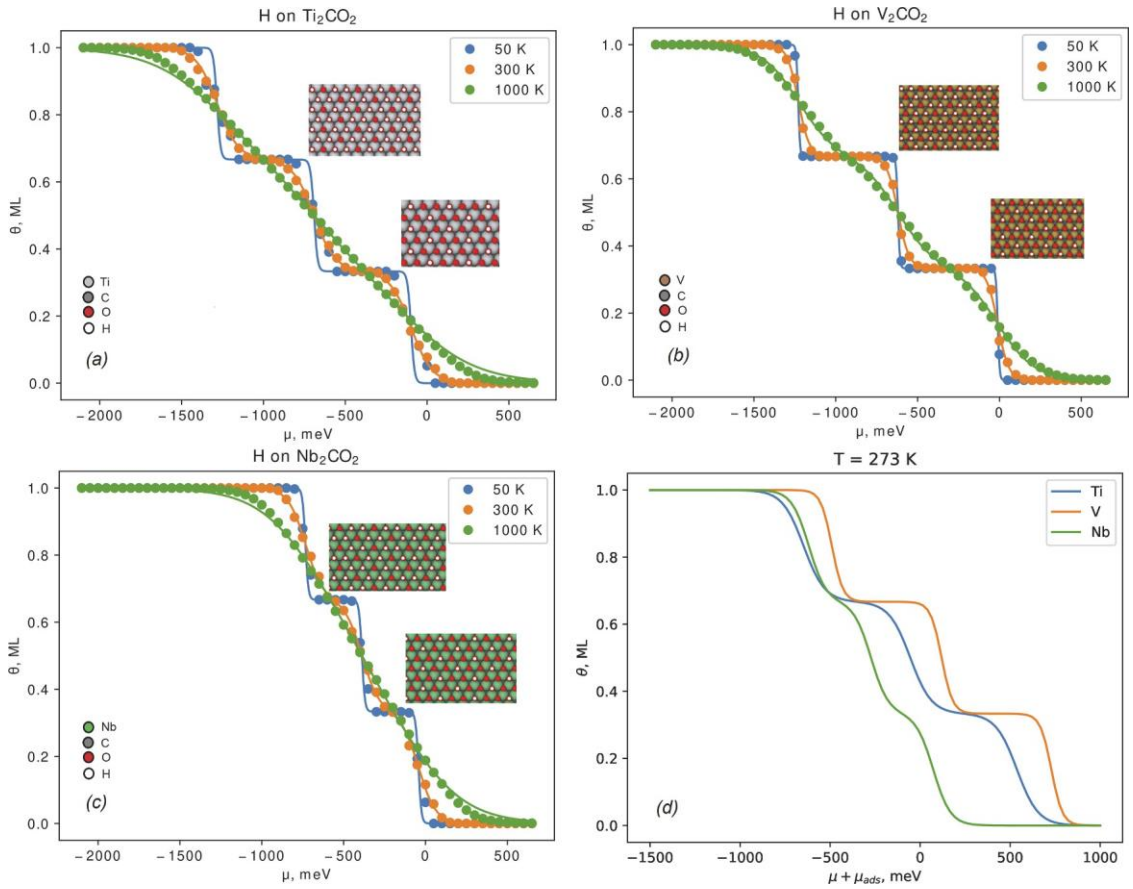

Fig. 2. Adsorption isotherms of hydrogen on MXenes M_2CO_2 (M = Ti, V, Nb). Circles - Monte Carlo simulated points, lines - approximations with Formula (8). (a)-(c) adsorption isotherms as functions of chemical potential relative to zero-coverage limit adsorption energy. (d) adsorption isotherms as functions of chemical potential including binding energy at T = 273 K.

Table 2
Parameters of isotherm approximations (Formula (8)).

	λ, meV	A	s, meV
Ti_2CO_2	691.02	0.40	592.63
V_2CO_2	620.04	0.77	609.64
Nb_2CO_2	387.93	0.49	345.48

isotherms using least squares approach.

Value of λ was calculated as a sum of lateral interactions $\Phi(r)$ weighted by coordination numbers of corresponding distances. It worth noting, that significant part of λ magnitude comes from further than nearest lateral interactions (up to 75% for Nb). That confirms importance of long-range interactions for quantitative modelling of even such a simple system.

From Figs. 2(a), 1(c) one can see that proposed approximations predict more rapid transitions between ordered phases at low temperature, than it is observed from simulations. In other cases, approxima- tion errors are less than 0.03 ML.

4. Conclusion

We have investigated the MXenes M_2CO_2 (M = Ti, V, Nb) surfaces reduction by hydrogen. Accurate and stable pairwise potential of lateral interactions between hydrogen adatoms was constructed and parameterized for each considered MXene. This potential is always repulsive. Nearest-neighbour repulsions negatively correlate with the lattice parameter. Repulsions between second-nearest neighbours is weaker than between third-nearest. Due to lateral interactions hydrogen adlayer on considered MXenes features ordered phases with 1/3 and 2/3 ML coverage and varying thermal stability. Long-range lateral interactions significantly influence on adsorptive properties of MXenes, shifting intermediate coverage region by about 0.3 eV. Generally, the Nb_2CO_2 MXene turned to be the weakest hydrogen adsorbent, and the V_2CO_2 is the strongest one. In atmospheric air at normal conditions it is expected that Nb_2CO_2 has near-zero hydrogen coverage, while on V_2CO_2 and Ti_2CO_2 hydrogen adlayer should form ordered phase with 1/3 ML coverage.

CRediT authorship contribution statement

Tatyana R. Kayumova: Methodology, Investigation, Visualization, Writing - review & editing. **Ilay P. Kolganov:** Validation, Visualization, Writing - review & editing. **Alexander V. Myshlyavtsev:** Software. **Pavel V. Stishenko:** Conceptualization, Methodology, Software, Writing - original draft, Writing - review & editing. **Anastasiia I. Fadeeva:** Supervision.

Declaration of Competing Interest

The authors declare that they have no known competing financial interests or personal relationships that could have appeared to influence the work reported in this paper.

Acknowledgements

This study was supported by the Ministry of Science and Higher Education of the Russian Federation on a budget-funded basis for

2020-2022 (project No FSGF-2020-0001).

References

[1] P. Lv, Y.L. Li, J.F. Wang, Monolayer Ti_2C MXene: manipulating magnetic properties and electronic structures by an electric field, Phys. Chem. Chem. Phys. 22 (2020) 11266-11272, https://doi.org/10.1039/D0CP00507J.

[2] Z. Fu, N. Wang, D. Legut, C. Si, Q. Zhang, S. Du, T.C. Germann, J.S. Francisco, R. Zhang, Rational design of flexible two-dimensional MXenes with multiple functionalities, Chem. Rev. 119 (2019) 11980-12031, https://doi.org/10.1021/acs.chemrev.9b00348.

[3] M. Khazaei, M. Arai, T. Sasaki, M. Estilic, Y. Sakkad, Two-dimensional molybdenum carbides: potential thermoelectric materials of the MXene family, Phys. Chem. Chem. Phys. 16 (2014) 7841-7849, https://doi.org/10.1039/C4CP00467A.

[4] B. Anasori, M.R. Lukatskaya, Y. Gogotsi, 2D metal carbides and nitrides (MXenes) for energy storage, Nat. Rev. Mater. 2 (2017) 16098, https://doi.org/10.1038/natrevmats.2016.98.

[5] B. Scheibe, J.K. Wychowaniec, M. Scheibe, B. Peplinska, M. Jarek, G. Nowaczyk, Ł. Przysiecka, Cytotoxicity assessment of Ti-Al-C Based MAX phases and $Ti_3C_2T_x$ MXenes on human fibroblasts and cervical cancer cells, ACS Biomater. Sci. Eng. (5) (2019) 6557-6569, https://doi.org/10.1021/acsbiomaterials.9b01476.

[6] Y. Wang, W. Tian, H. Zhanga, Y. Wang, Nb_2N monolayer as a promising anode material for Li/Na/K/Ca-ion batteries: a DFT calculation, Phys. Chem. Chem. Phys. 23 (2021) 12288-12295, https://doi.org/10.1039/D1CP00993A.

[7] S. Zhanga, W.Q. Han, Recent advances in MXenes and their composites in lithium/sodium batteries from the viewpoints of components and interlayer engineering, Phys. Chem. Chem. Phys. 22 (2020) 16482-16526, https://doi.org/10.1039/D0CP02275F.

[8] M.Q. Zhao, C.E. Ren, M. Alhabeb, B. Anasori, M.W. Barsoum, Y. Gogotsi, Magnesium-Ion Storage Capability of MXenes, ACS Appl. Energy Mater. 2 (2019) 1572-1578, https://doi.org/10.1021/acsaem.8b02253.

[9] E.M.D. Siriwardane, I. Demiroglu, C. Sevik, F.M. Peeters, D. Çakır, Assessment of sulfur-functionalized MXenes for Li-ion battery applications, J. Phys. Chem. C 124 (2020) 21293-21304, https://doi.org/10.1021/acs.jpcc.0c05287.

[10] A. Mohan T, N. Kuriakose, K. Mondal, P. Ghosh, CO_2 capture, activation and dissociation on the Ti_2C surface and Ti_2C MXene: the role of surface structure, Phys. Chem. Chem. Phys. 22 (2020) 14599-14612, https://doi.org/10.1039/D0CP01700K.

[11] H. Nam, E.S. Sim, M. Je, H. Choi, Y.C. Chung, Theoretical Approach toward Optimum Anion-Doping on MXene Catalysts for Hydrogen Evolution Reaction: an Ab Initio Thermodynamics Study, ACS Appl. Mater. Interfaces 13 (2021) 37035-37043, https://doi.org/10.1021/acsami.1c07476.

[12] Z. Lv, W. Ma, J. Dang, M. Wang, K. Jian, D. Liu, D. Huang, Ultra-narrow-band NIR photomultiplication organic photodetectors based on charge injection narrowing, J. Phys. Chem. Lett. 12 (2021) 4841-4848, https://doi.org/10.1021/acs.jpclett.1c00330.

[13] J. Zhao, L. Zhang, X.Y. Xie, X. Li, Y. Ma, Q. Liu, W.H. Fang, X. Shi, G. Cui, X. Sun, $Ti_3C_2T_x$ (T = F, OH) MXene nanosheets: conductive 2D catalysts for ambient electrohydrogenation of N_2 to NH_3, J. Mater. Chem. A 6 (2018) 24031-24035, https://doi.org/10.1039/C8TA09840A.

[14] X. Lv, L. Kou, T. Frauenheim, Catalytic effect on CO_2 electroreduction by hydroxyl-terminated two-dimensional MXenes, ACS Appl. Mater. Interfaces 13 (2021) 14283-14290, https://doi.org/10.1021/acsami.9b09941.

[15] M.A. Hope, A.C. Forse, K.J. Griffith, M.R. Lukatskaya, M. Ghidiu, Y. Gogotsi, C. P. Grey, NMR reveals the surface functionalisation of Ti_3C_2 MXene, Phys. Chem. Chem. Phys. 18 (2016) 5099-5102, https://doi.org/10.1039/C6CP00330C.

[16] T. Kobayashi, Y. Sun, K. Prenger, D. Jiang, M. Naguib, M. Pruski, Nature of terminating hydroxyl groups and intercalating water in $Ti_3C_2T_x$ MXenes: a study by 1H solid-state NMR and DFT calculations, J. Phys. Chem. C 124 (2020) 13649-13655, https://doi.org/10.1021/acs.jpcc.0c0474.

[17] X.H. Li, L. Shan-Shan, H.L. Cui, R.Z. Zhang, Pressure-induced modulation of electronic and optical properties of surface O-functionalized Ti_2C MXene, ACS Omega 5 (2020) 22248-22254, https://doi.org/10.1021/acsomega.0c02435.

[18] C. He, Q. Zhao, Y. Huang, W. Du, L. Zhu, Y. Zhou, S. Zhanga, X. Xu, Strain-dependent anisotropic nonlinear optical response in two-dimensional functionalized MXene Sc_2CT_2 (T = O and OH), Phys. Chem. Chem. Phys. 22 (2020) 21428-21435, https://doi.org/10.1039/D0CP03968C.

[19] Q.D. Chen, S.F. Yuan, J.H. Dai, Y. Song, Functionalized $M_2TiC_2T_x$ MXenes (M = Cr and Mo; T = F, O, and OH) as high performance electrode materials for sodium ion batteries, Phys. Chem. Chem. Phys. 23 (2021) 1038-1049, https://doi.org/10.1039/D0CP01846E.

[20] R. Ibragimova, M.J. Puska, H.-.P. Komsa, pH-dependent distribution of functional groups on titanium-based MXenes, ACS Nano 13 (2019) 9171-9181, https://doi.org/10.1021/acsnano.9b03511.

[21] I. Persson, L.Å. Näslund, J. Halim, M.W. Barsoum, V. Darakchieva, J. Palisaitis, J. Rosen, P.O.Å. Persson, On the Organization and Thermal Behavior of Functional Groups on Ti3C2 MXene Surfaces in Vacuum, 2D Mater. 5 (2018) 015002. 10.1088/2053-1583/aa89cd.

[22] P.V. Stishenko, T.R. Kayumova, A.V. Myshlyavtsev, Phase behavior of terminating oxygen layer of V_2C MXene, in: Proceedings of the AIP Conference 2285, 2020, 020020, https://doi.org/10.1063/5.0026690.

[23] X. Ren, M. Huo, M. Wang, H. Lin, X. Zhang, J. Yin, Y. Chen, H. Chen, Highly catalytic niobium carbide (MXene) promotes hematopoietic recovery after radiation by free radical scavenging, ACS Nano 13 (2019) 6438-6454, https://doi.org/10.1021/acsnano.8b09327.

[24] J. Hu, B. Xu, C. Ouyang, S.A. Yang, Y. Yao, Investigations on V_2C and V_2CX_2 (X = F, OH) monolayer as a promising anode material for Li ion batteries from first-principles calculations, J. Phys. Chem. C 118 (2014) 24274-24281, https://doi.org/10.1021/jp507336x.

[25] Q. Zhang, X. Zhang, Y. Xiao, C. Li, H.H. Tan, J. Liu, Y. Wu, Theoretical insights into the favorable functionalized Ti_2C-Based MXenes for lithium sulfur batteries, ACS Omega 5 (2020) 29272-29283, https://doi.org/10.1021/acsomega.0c04043.

[26] P. Giannozzi, S. Baroni, N. Bonini, et al., QUANTUM ESPRESSO: a modular and open-source software project for quantum simulations of materials, J. Phys. Condens. Matter. 21 (2009), 395502, https://doi.org/10.1088/0953-8984/21/39/395502.

[27] S.S. Akimenko, G.D. Anisimova, A.I. Fadeeva, V.F. Fefelov, V.A. Gorbunov, T. R. Kayumova, A.V. Myshlyavtsev, M.D. Myshlyavtseva, P.V. Stishenko, SuSMoST: surface science modeling and simulation toolkit, J. Comput. Chem. 41 (2020) 2084-2097, https://doi.org/10.1002/jcc.26370.

[28] S. Grimme, J. Antony, S. Ehrlich, H. Krieg, A consistent and accurate ab initio parametrization of density functional dispersion correction (DFT-D) for the 94 elements H-Pu, J. Chem. Phys. 132 (2010), 154104, https://doi.org/10.1063/1.3382344.

[29] F.O. Sanchez-Varretti, P.M. Pasinetti, F.M. Bulnes, A.J. Ramirez-Pastor, Adsorption of binary mixtures on two-dimensional triangular lattices, Surf. Sci. 701 (2020), 121698, https://doi.org/10.1016/j.susc.2020.121698.

[30] J.B. Collins, P.A. Rikvold, E.T. Gawlinski, Finite-size scaling analysis of the S=1 Ising model on the triangular lattice, Phys. Rev. B 38 (1988) 6741-6750, https://doi.org/10.1103/PhysRevB.38.6741.

[31] C. Zhan, M. Naguib, M. Lukatskaya, P.R.C. Kent, Y. Gogotsi, D. Jiang, Understanding the MXene Pseudocapacitance, J. Phys. Chem. Lett. 9 (2018) 1223-1228, https://doi.org/10.1021/acs.jpclett.8b00200.

[32] U. Schmidt, Geology, molecular hydrogen in the atmosphere, Tellus A 26 (1974) 78-90, https://doi.org/10.1111/j.2153-3490.1974.tb01954.x.